Quantification and Assessment of Global Terrestrial Water Storage Deficit Caused by Drought Using GRACE Satellite Data

Jing Lu, Li Jia, *Member, IEEE*, Jie Zhou, Min Jiang, Yulong Zhong, and Massimo Menenti

***Abstract*—A drought-induced water storage deficit index (D-WSDI) is proposed to quantify the response of GRACE-based terrestrial water storage change to meteorological drought and the impact of drought on water storage deficit. D-WSDI is defined as the normalized residual component of GRACE time-series data after removing the long-term trend and seasonal components. The evaluation based on the Emergency Events Database (EM-DAT) showed that more than 90% of global drought events from 2002 to 2019 led to a water storage deficit, which can be detected by the proposed D-WSDI. The severity of the water storage deficit caused by drought increases with the extending drought duration. An average of 73% of water storage deficit months at the global scale is related to precipitation shortages. The cumulative precipitation deficit in relatively short periods of less than 9 months can lead to the water storage deficit in low-latitude regions, whereas a longer time scale is required to lead to a water storage deficit in high-latitude regions. The negative monthly precipitation anomaly of about −20% can lead to a water storage deficit in high rainfall regions, whereas the negative precipitation anomaly can reach −80% in arid and semiarid areas. D-WSDI holds the capability to quantify the water storage deficit caused by drought, especially in the regions with terrestrial water storage change influenced by the long-term trends in climate and anthropogenic activities, and can be used as an index of drought monitoring with similar or superior performance compared to some traditional drought indices.**

***Index Terms*—Decomposing time series, drought, Gravity Recovery and Climate Experiment (GRACE), water storage deficit.**

Manuscript received January 29, 2022; revised May 5, 2022; accepted May 26, 2022. Date of publication June 8, 2022; date of current version June 29, 2022. This work was supported by the Strategic Priority Research Program of the Chinese Academy of Sciences under Grant XDA19030203 and in part by the Open Fund of State Key Laboratory of Remote Sensing Science under Grant OFSLRSS202107. The work of Massimo Menenti was supported in part by the Chinese Academy of Sciences President's International Fellowship Initiative under Grant 2020VTA0001 and in part by the MOST High-Level Foreign Expert Program under Grant GL20200161002. *(Corresponding author: Jing Lu.)*

Jing Lu, Li Jia, and Min Jiang are with the State Key Laboratory of Remote Sensing Science, Aerospace Information Research Institute, Chinese Academy of Sciences, Beijing 100101, China (e-mail: lujing@aircas.ac.cn; jiali@aircas.ac.cn; jiangmin@aircas.ac.cn).

Jie Zhou is with the School of Urban and Environmental Sciences, Central China Normal University, Wuhan 430079, China (e-mail: zhou.j@ccnu.edu.cn).

Yulong Zhong is with the School of Geography and Information Engineering, China University of Geosciences (Wuhan), Wuhan 430074, China (e-mail: zhongyl@cug.edu.cn).

Massimo Menenti is with the State Key Laboratory of Remote Sensing Science, Aerospace Information Research Institute, Chinese Academy of Sciences, Beijing 100101, China, and also with Delft University of Technology, 2628 CD Delft, The Netherlands (e-mail: m.menenti@tudelft.nl).

This article has supplementary downloadable material available at https://doi.org/10.1109/JSTARS.2022.3180509, provided by the authors.

Digital Object Identifier 10.1109/JSTARS.2022.3180509

Nomenclature

D-WSDI	Drought-induced water storage deficit index.
DRC	Democratic Republic of the Congo.
DSI	GRACE-based Drought Severity Index.
EM-DAT	Emergency Events Database.
GHDI	GRACE-based Hydrological Drought Index.
GPCC	Global Precipitation Climatology Centre.
GPCP	Global Precipitation Climatology Project.
GPM	Global Precipitation Measurement.
GRACE	Gravity Recovery and Climate Experiment.
GRACE-FO	GRACE Follow-On.
IMERG	Integrated Multi-SatellitE Retrievals for GPM.
MTWSDI	Modified the total water storage deficit index.
PAP	Precipitation anomaly percentage.
scPSDI	Self-calibration Palmer Drought Severity Index.
SPEI	Standard precipitation evapotranspiration index.
SPI	Standard precipitation index.
TSDI	Total storage deficit index.
TWS	Terrestrial water storage.
TWSA	TWS anomaly.
WSDI	Water storage deficit index.

I. Introduction

THE terrestrial water storage (TWS), including surface water, soil moisture, groundwater, canopy water content, snow, ice, and permafrost, is an integrated measure of water availability and the terrestrial freshwater stock. As a status indicator of the water cycle, the variations of TWS are related to climate change, hydrological extremes, and human activities [1], [2]. However, it is difficult to measure TWS due to the lack of complete *in situ* observations of the terrestrial water cycle components [3], [4]. The Gravity Recovery and Climate Experiment (GRACE) mission, launched in March 2002, provides measurements of the spatial-temporal changes in Earth's gravity field. GRACE observations have been used in the cryosphere, hydrology, and ocean sciences to monitor the terrestrial water cycle, ice sheet and glacier mass balance, sea-level change, and ocean bottom pressure variations to respond to global climate system changes, which has important implications for global water, food, and human security [5], [6].

As a climate extreme, drought usually occurs due to the persistent shortage of water, which can lead to changes in surface

This work is licensed under a Creative Commons Attribution-NonCommercial-NoDerivatives 4.0 License. For more information, see https://creativecommons.org/licenses/by-nc-nd/4.0/

variables related to the water cycle and trigger the regional or global water and food crisis [7]. Satellite-derived variables associated with water and vegetation have been used to develop various drought indices for drought monitoring and assessment, including precipitation-based indices, evapotranspiration-based indices, vegetation-based indices, land surface temperature-based indices, soil moisture-based indices, snow-based indices, groundwater and TWS-based indices, and the integrated indices [8], [9]. The GRACE satellite mission provides an alternative approach to monitoring drought from an integrated perspective. It can detect vertically integrated water storage changes from the land surface to the deepest aquifers [10]. A large number of studies used GRACE TWS anomaly (TWSA) for drought monitoring and evaluation, especially for hydrological drought [11]–[17]. Some drought indices based on GRACE data have also been proposed to provide hydrologists with practical insights into integrated drought indices, including the total storage deficit index (TSDI), the GRACE-based hydrological drought index (GHDI), the GRACE-based Drought Severity Index (DSI), the water storage deficit index (WSDI), etc. [18]–[22].

TWS deficit is closely related to drought but is not the only factor triggering drought. Thomas *et al.* [23] provided a quantitative storage deficit method for measuring hydrological drought occurrence and severity using TWS measurements from the GRACE satellite. This method used GRACE measurements to calculate the magnitude of regional monthly TWS anomalies from the time-series monthly climatology, and the negative deviations of the monthly climatology represent storage deficits. The GRACE-based drought indices mentioned above, with a similar principle to the method presented in [23], can be used to quantify the water storage deficit caused by meteorological drought. However, one major issue with the existing GRACE-based drought indices is the existence of long-term trends in some regions, for instance, groundwater depletion, storage of water, and glacier retreat, which may not be caused by drought [15], [16], [24]–[27]. If the long-term trend is not eliminated, the GRACE-based drought indices will inevitably provide unreliable information on the impact of drought on water storage. Based on the approach presented in [23], Humphrey *et al.* [24] assessed global trends, seasonal cycles, subseasonal anomalies, and hydrological extremes in TWS from GRACE data. The notable linear trend can result in one end of the time-series systematically above/below the seasonal cycle. Using the residual signal after removing the deterministic behavior of the time series instead of the total signal, Hosseini-Moghari *et al.* [25] modified the TSDI index to monitor drought in the Markazi Basin of Iran. The results were consistent with the standard precipitation index (SPI) and the standard precipitation evapotranspiration index (SPEI). Liu *et al.* [27] showed that GRACE-based DSI computed with the detrended GRACE-TWS time series reasonably captures the drought process in China compared to existing drought indices based on nondetrended GRACE data. The modified MTWSDI removed the long-term trend in GRACE time-series data, separating meteorological variability from anthropogenic impacts on water availability [26]. These studies paid more attention to GRACE-based drought monitoring at regional sales or the major river basins. In the review of drought monitoring applications based on GRACE observations, Yi and Wen [16] pointed out that each drought index can characterize/analyze drought with excellent efficacy in a specifical case study. Still, their global performance is questioned from time to time because of the complexity of the process.

Many factors can influence the water storage deficit. This study will mainly focus on quantifying and assessing the global water storage deficit caused by drought using TWS change from GRACE data product and drought event information extracted from the Emergency Events Database (EM-DAT). The specific objectives of this article include the following:

1) to propose a GRACE-based drought-induced water storage deficit index (D-WSDI) by using the time-series decomposition method to quantify the water storage deficit caused by drought;
2) to explore the probability that drought led to water storage deficit;
3) to clarify the magnitude and duration of precipitation anomaly that would lead to water storage deficit;
4) to compare D-WSDI with other commonly used drought indices for drought detection.

II. Data

A. GRACE/GRACE-FO Monthly Mass Grids Data

GRACE mission measured mass changes of the Earth every month from April 2002 through June 2017. GRACE Follow-On (GRACE-FO) has continued this data record since June 2018. The assessment of the global mass change fields through December 2019 has demonstrated that GRACE-FO is extending the original GRACE record at an equivalent precision and spatiotemporal sampling [28]. Fatolazadeh and Goïta [29] also showed that TWS changes and their uncertainties derived by GRACE-FO are consistent with GRACE estimates. The GRACE/GRACE-FO satellite observations can be used to derive monthly gravity field variation by a complex inversion. Mass concentration blocks (mascons) are essentially another solution for GRACE satellite data different from a spherical harmonic method, with higher accuracy and potential for hydrologic applications [10], [30]. Monthly Mass Grids-Global mascons processed by GRCTellus JPL (JPL RL06_v02) with 0.5° global grids from 2002 to 2019,[1] was used in this study. For the missing data in this dataset due to GRACE battery management and a one-year gap between GRACE and GRACE-FO data, many methods have been developed to fill the gaps so that the consecutive and coherent data can be generated for more applications in hydrology and water resources [28], [31]–[33]. This study used the publicly released reconstructed data based on JPL mascon and ERA5 data from Humphrey and Gudmundsson [31] to fill the missing data in JPL RL06_v02 data, including January to March of 2002. The reconstructed data have a consistent data source with JPL RL06_v02 data and are often superior to those driven by other precipitation datasets. The based-precipitation reconstruction removed the seasonal precipitation cycle without removing the long-term trend, while the GRACE/GRACE-FO data had the long-term and seasonal trends. Therefore, the

[1] [Online]. Available: http://grace.jpl.nasa.gov

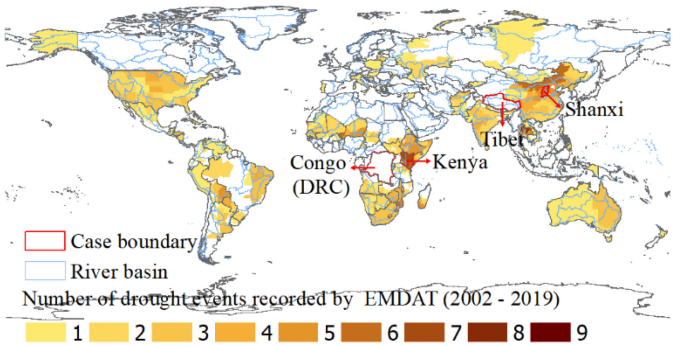

Fig. 1. Number of drought events from the EM-DAT database during 2002–2019 disaggregated by province.

detrended reconstructed data were first done and then used to fill the JPL RL06_v02 missing data after detrending and deseasonalizing.

B. Global Drought Events From EM-DAT Database

EM-DAT was launched by the Centre for Research on the Epidemiology of Disasters with the initial support of the World Health Organization and the Belgian Government for humanitarian action at national and international levels.[2] The database is compiled from various sources, including U.N. agencies, nongovernmental organizations, insurance companies, research institutes, and press agencies. It contains essential core data on the occurrence and effects of over 22 000 massive disasters, including drought, flood, extreme temperature, wildfire, earthquake, volcanic activity, epidemic, etc., in the world from 1900 to the present day. EM-DAT database records drought events as the climatological extreme. Although the EM-DAT database cannot cover all drought events, the recorded drought events are indeed the happened droughts. The onset month, termination month, and locations of global drought events from 2002 to 2019 are extracted from the EM-DAT database. There are 289 drought records in the EM-DAT database from 2002 to 2019, covering 97 countries and 1332 subnational (provincial) administerial units. At the provincial scale, there are 2563 drought events. Fig. 1 shows that the drought frequently occurred in eastern Africa, such as Ethiopia and Kenya (related to the Nile River Basin), southern Africa (including the Zambezi River Basin), Thailand (the downstream Mekong River Basin), Northern China (involved to Yellow River Basin, Hai River Basin, and Liao River Basin), America, and Amazon basin in South America. All drought records at the provincial scale were binned into four drought duration classes, i.e., 1 to 3 months, 4 to 6 months, 7 to 12 months, and longer than 12 months. The percentage of drought records in each class was 27%, 23%, 31%, and 19%, respectively.

C. GPM Monthly Precipitation Data

The Global Precipitation Measurement (GPM) mission is a joint satellite mission led by NASA and JAXA. GPM core observatory satellite was launched in February 2014, with advanced spaceborne active and passive sensors for accurate retrievals of rainfall and snowfall. The Integrated Multi-SatellitE Retrievals for GPM (IMERG) algorithm developed by the U.S. Science Team is used to generate the best precipitation estimates at 0.1° every half hour globally [34], [35]. The precipitation estimates are from the various precipitation-relevant satellite passive microwave sensors comprising the GPM constellation and also have been adjusted with the monthly GPCP Satellite-Gauge (S.G.) product. GPM IMERG Final Precipitation L3 1 month 0.1° × 0.1° V06 (GPM_3IMERGM) product,[3] is used in this study. To match the spatial resolution of GRACE data, the GPM precipitation data in this study were aggregated to 0.5°. The upscaled GPM precipitation data are in excellent agreement with the Global Precipitation Climatology Centre's 0.5° monthly precipitation (GPCC Full Data Monthly Product Version 2020 at 0.5°[4]), with $r > 0.9$ and the relative bias less than 20% for most world regions. The comparison results are shown in Fig. S1 of supplementary materials. The slight inconsistency is only found in part regions of North Africa and the high-latitude areas of the Northern Hemisphere. The prolonged precipitation shortage is the primary reason for most drought events. The GPM precipitation data were used to assess the reliability of these drought records in the EM-DAT database and analyze the relationship between precipitation deficit and water storage deficit.

D. Drought Indices scPDSI and SPEI Data

The scPSDI based on climatic and environmental parameters is a variant of the original PDSI of Palmer [36] and was introduced by Wells *et al.* [37]. The scPDSI is calculated from time series of precipitation and temperature, together with fixed parameters related to the soil/surface characteristics at each location to make results from different climate regimes more comparable [38]. The monthly scPDSI data at the spatial resolution of a 0.5° grid based on the CRU-TS-4.04 (Climatic Research Unit Time-Series version 4.04 of high-resolution gridded data of month-by-month variation in climate)[5] were used in this study. The value of −0.5 is commonly regarded as the threshold value of scPDSI to identify drought.

SPEI expresses the deviations of precipitation minus potential evapotranspiration to the long-term average. SPEI is similar to SPI with the advantage of multiscale character, but it includes the effects of temperature variability on drought assessment [39]. The Global 0.5° gridded SPEI dataset[6] was used in this study to provide drought information across multiscale between 1 and 24 months. SPEI <0 is classified as drought at different severity levels.

[2][Online]. Available: https://www.emdat.be

[3][Online]. Available: https://gpm1.gesdisc.eosdis.nasa.gov/data/GPM_L3/GPM_3IMERGM.06/

[4][Online]. Available: https://opendata.dwd.de/climate_environment/GPCC/html/fulldata-monthly_v2020_doi_download.html

[5][Online]. Available: https://crudata.uea.ac.uk/cru/data/drought/

[6][Online]. Available: http://digital.csic.es/handle/10261/153475

III. Methods

A. Drought-Induced Water Storage Deficit Index (D-WSDI) by Decomposing Time-Series Method

The additive decomposition method [40] was used to decompose the GRACE time-series data (S_{total}) into the three components, i.e.,

$$S_{\text{total}} = S_{\text{long-term}} + S_{\text{seasonal}} + Residuals \tag{1}$$

where $S_{\text{long-term}}$ is the deterministic and nonseasonal long-term trend component, S_{seasonal} is the deterministic seasonal component with known periodicity, and $Residuals$ is the stochastic irregular component. A linear model and a stable seasonal filter with 12 months [41] are used to obtain the long-term trend and the seasonal component in this study. A stable seasonal filter assumes that the seasonal level is constant over the range of the data. The detail for the stable seasonal filter is given in Appendix. The $Residuals$ is the residual part of the time-series data after removing the long-term and the seasonal components, which is usually the most useful component for short-term variation detection. In this method, the interannual change component in time-series data is not considered separately and included in $Residuals$. The negative anomaly of the $Residuals$ is suitable for measuring the impact of drought on TWS.

Normalization can provide an indicator easier to compare across geographical regions. The D-WSDI was thus defined as the ratio of the $Residuals$ in GRACE time-series data to its standard deviation (δ) according to the following equation:

$$\text{D}-\text{WSDI} = \frac{Residuals}{\delta\left(Residuals\right)}. \tag{2}$$

We used the standard deviation rather than the difference of maximum and minimum in (2) to normalize the D-WSDI to avoid the impacts of the extreme maximum and minimum on the results. In addition, unlike previously WSDI defined by Sun *et al.* [22], we did not subtract the mean value of $Residuals$ in the numerator because detrending implied the operation. The purpose of this operation without deducting the mean value in this study is to hold that D-WSDI has the same implication with $Residuals$, i.e., D-WSDI < 0 means that drought causes the reduction of TWS. The smaller the D-WSDI value, the more severe impacts of droughts on TWS.

B. Sun's WSDI and Zhao's DSI

Sun *et al.* [22] defined the WSDI to evaluate drought severity over the Yangtze River Basin of China (hereinafter referred to as Sun's WSDI). In Sun's method, WSDI is defined as follows:

$$\text{WSDI} = \frac{\text{WSD} - \overline{\text{WSD}}}{\delta\left(\text{WSD}\right)}$$

$$\text{with } WSD_{i,j} = \text{TWSA}_{i,j} - \overline{\text{TWSA}_j} \tag{3}$$

where $\text{TWSA}_{i,j}$ is the GRACE-based TWSA in the *j*th month of year *i*. $\overline{\text{TWSA}_j}$ is the long-term mean of TWSA in month *j*. WSDI < 0 is the criterion to identify drought.

The DSI developed by Zhao *et al.* [20], [21] was defined as:

$$\text{DSI} = \frac{\text{TWSA}_{i,j} - \overline{\text{TWSA}_j}}{\delta\left(\text{TWSA}_j\right)} \tag{4}$$

where $\delta(\text{TWSA}_j)$ is the standard deviation of TWSA in month *j*. DSI <-0.5 is the criterion to monitor drought.

C. Precipitation Anomaly Percentage (PAP)

PAP presents the precipitation anomaly as a percentage of the long-term average for a specific period, which is expressed as follows:

$$\text{PAP} = \frac{P - \bar{P}}{\bar{P}} \times 100\%$$

where *P* is the accumulated precipitation during a specified period, and $\bar{P}$ is the long-term average of accumulated precipitation of the same period. The negative PAP represents that accumulated precipitation is less than the historical average during the specified period. Negative PAP quantifies the precipitation deficit.

D. Evaluation Metrics

Two main evaluation metrics, i.e., the consistency percentage (*cp*) and the correlation coefficient (*r*), are used to quantify the assessment accuracy of the response of D-WSDI to global drought events and precipitation deficit and the relationships between D-WSDI and other drought indices. The consistency percentage is similar to the probability of detection [42], which is expressed as:

$$cp = \frac{n2\left(x \in \text{c1} \cap y \in \text{c2}\right)}{n1\left(x \in \text{c1}\right)} \times 100\% \tag{5}$$

where *x* and *y* are two variables with *n* elements. $n1$ is the number of occurrences such as $x \in c1$, whereas $n2$ is the number of occurrences such as $x \in c1 \cap y \in c2$. $c1$ and $c2$ are the different criteria for the two independent variables.

cp mainly quantified the response of D-WSDI to global drought events. The percentage of all EM-DAT drought events with D-WSDI < 0 expresses the likelihood that EM-DAT drought events may lead to a water storage deficit. The percentage of D-WSDI in response to the duration of the EM-DAT drought events is the portion of months with D-WSDI < 0, indicating how long the water storage deficit is caused by drought. The percentage of the area with D-WSDI < 0 to the total extent of a simultaneous EM-DAT drought event in the same region is a metric of the spatial response of TWS to drought. In the early stage of a drought event, the area affected by drought is limited. With the evolution of the drought, the area affected by drought may first expand and then decrease. The maximum affected area in the drought process was a spatial indicator of drought severity. The percentage of the months of D-WSDI < 0 with PAP < 0 to all months of D-WSDI < 0 is used to quantify the intensity of the water storage deficit related to the precipitation deficit, also the consistency between PAP and negative D-WSDI.

E. Overall Framework

The overall technique flowchart of this study is shown in Fig. 2. To realize the objective of quantifying and assessing the global water storage deficit caused by drought, the main works of this study are to develop the D-WSDI index, to evaluate its response to drought event characteristics, to explore the relationship between water storage deficit caused by drought

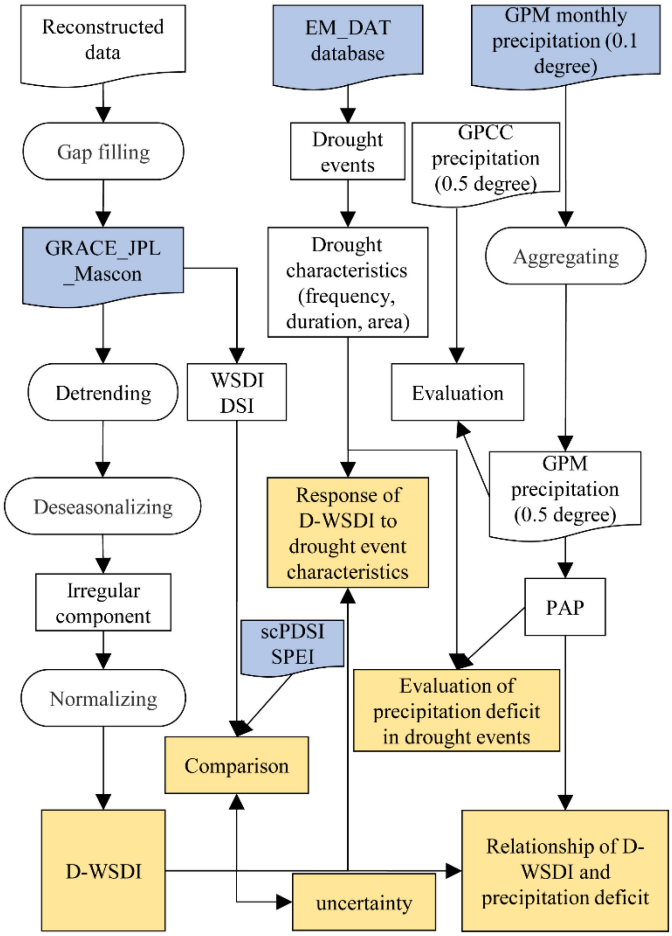

Fig. 2. Overall technique flowchart of this study.

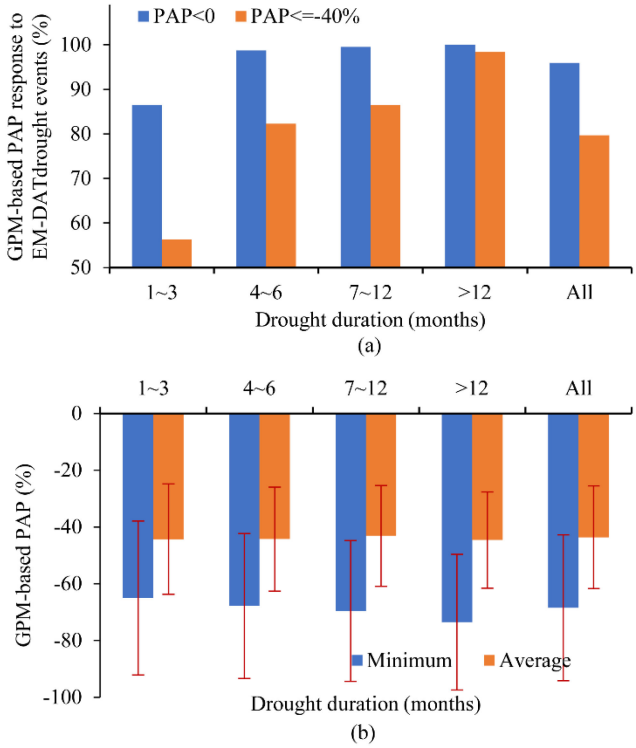

Fig. 3. (a) Percentage of GPM-based PAP response to drought events from the EM-DAT database. (b) Average and minimum of PAP.

and precipitation deficit, and to compare D-WSDI with other drought indices further to clarify the performance of D-WSDI for drought detection. In addition, the uncertainties of D-WSDI from different schemes of detrending and deseasonalizing are also analyzed. All results are given in Section IV.

IV. Results and Discussion

A. Response of D-WSDI to EM-DAT Global Drought Events

1) Precipitation Deficit in Global Drought Events: PAP is a simple climate-based drought index widely used to evaluate meteorological drought [43]. In China, a meteorological drought is defined by a monthly PAP $<=-40\%$ [44]. According to this definition, 80% of the EM-DAT drought events fall in this category. The fraction increases with increasing drought duration, 56% for drought events of 1 to 3 months, and 98% for drought events longer than 12 months [see Fig. 3(a)]. PAP $<=-40\%$ as a meteorological drought is spatial dependence, which can differ with regions. In nearly all EM-DAT drought events, about 96% are associated with PAP < 0. The mean PAP for all EM-DAT drought events is -44%, with a standard deviation of 18%, indistinctive change with drought duration. The mean of the minimum PAP during the EM-DAT drought events is -68%, with a standard deviation of 26%, and the magnitude of PAP negatively increases with increasing the drought duration [see Fig. 3(b)]. A few drought events without negative precipitation anomaly can be attributed to counting at the province scale, especially for the provinces at the edge of the drought center, with not very severe droughts. Besides, the uncertainties from GPM precipitation data and the EM-DAT database may also influence the results.

2) Response of D-WSDI to Different Drought Characteristics: Fig. 4(a) shows that 92% of the EM-DAT drought events were associated with a detectable water storage deficit, i.e., at least one monthly negative D-WSDI. The percentage increases with increasing drought duration, 82% for short-term drought events lasting 1 to 3 months, and 98% for long-term drought events lasting more than one year. The D-WSDI has a significantly larger probability to identify drought events than other drought indices such as scPDSI, sun's WSDI, and Zhao's DSI, but slightly less than SPEI at the optimal time scale. The higher probability of long-term drought means that the long-term drought is more likely to reduce TWS. The lower percentage of short-term droughts can be attributed to two reasons. One is that the drought event is not severe enough to cause changes in TWS. The other is that the hydrological droughts commonly lag meteorological droughts, that is, water storage deficit lags precipitation deficit.

The average percentage of drought durations detected by D-WSDI is 75% of those recorded in EM-DAT [see Fig. 4(b)]. It means that about three fourth of the drought duration has a water storage deficit. The percentage is generally greater than other drought indices except for scPDSI. Since scPDSI is a

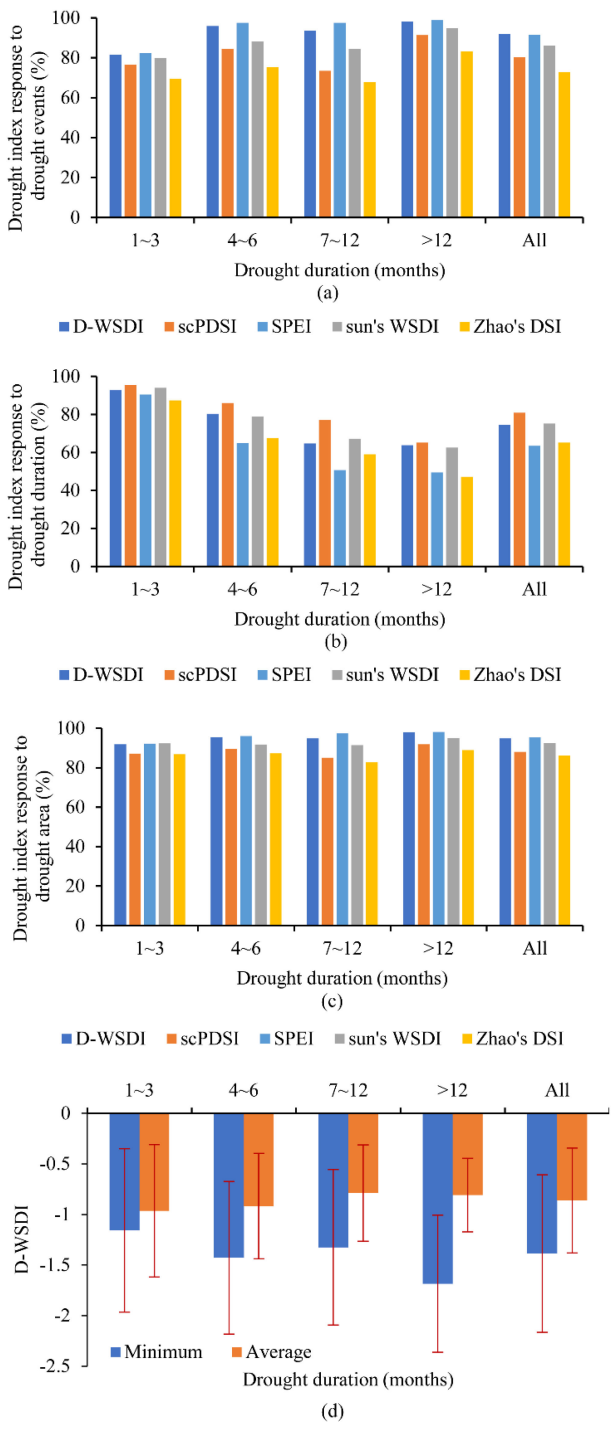

Fig. 4. Response of D-WSDI and other drought indices to drought characteristics with different durations: (a) the number of drought events, (b) drought duration, (c) drought area, and (d) the mean and minimum D-WSDI during EM-DAT drought events.

meteorological drought index, it is not strange that scPDSI is more consistent with the EM-DAT drought events reflecting the meteorological drought. With drought duration increasing, the percentage of duration detected by D-WSDI decreases. For the long-term drought, the percentage of D-WSDI detected duration is 64%, which might be due to D-WSDI > 0 in some months during an extended period. Interestingly, D-WSDI is higher, namely about 93%, for shorter drought events, which means that D-WSDI can capture fast responses to drought.

The percentage of the maximum drought area detected by D-WSDI to the drought area recorded by EM-DAT is above 90%, especially for long-term drought, the percentage can reach 98% [see Fig. 4(c)]. The result for drought area detection is also better than other drought indices, which means that D-WSDI can respond to drought well at the spatial distribution.

The minimum D-WSDI value during the duration of a drought event is an indicator of the severity of the water storage deficit caused by drought. The smaller the minimum, the more severe the water storage deficit caused by drought is. The mean D-WSDI during a drought event indicates the intensity of the water storage deficit caused by drought [see Fig. 4(d)]. The minimum D-WSDI value for the short-term drought events of 1 to 3 months was -1.2. Its absolute value grows with increasing drought duration with a D-WSDI $= -1.7$ for drought events over 12 months, further illustrating that more extended drought events lead to a more severe water storage deficit. The absolute value of mean D-WSDI decreases with increasing drought duration, a different trend from the minimum D-WSDI. However, the total water storage deficit cannot decrease due to the prolonged drought duration. The standard deviation of the minimum and mean D-WSDI for each drought class shows that even though the drought events may belong to the same duration, the severity and intensity of the water storage deficit caused by drought may differ.

B. Relationship of Water Storage Deficit Caused by Drought and Precipitation Deficit

1) Consistency of Negative D-WSDI and Precipitation Deficit at Different Time Scales: D-WSDI eliminated the long-term trend in GRACE data. Thus the water storage deficit caused by drought should mainly be driven by precipitation shortage during a certain period. The percentage of the months of negative D-WSDI and PAP to all months of negative D-WSDI was used to quantify the consistency of water storage deficit caused by drought and precipitation deficit. PAP at different time scales was calculated by the cumulative precipitation during the past 1 to 24 months. Only the months of D-WSDI < 0 lasting more than 3 months were counted. More than 60% of months with D-WSDI < 0 are simultaneous with PAP < 0 at different time scales for the majority (94%) of the world regions, and the mean percentage of the global is 73% [see Fig. 5(a)]. It means that 73% of water storage deficit duration is related to precipitation shortages. This result is very consistent with the result shown in Fig. 4(b): 75% of drought duration have a water storage deficit. Those regions with relatively low percentages are generally located in the high-latitude regions of the Northern Hemisphere and several islands in Southeast Asia. The main reasons can be attributed to two aspects. One is the uncertainty in precipitation data in high-latitude regions because it is always challenging to retrieve solid precipitation by remote sensing [34]. The other is that caution should be applied in the interpretation of GRACE data in ice-covered regions and land/ocean boundaries because of significant leakage errors [30].

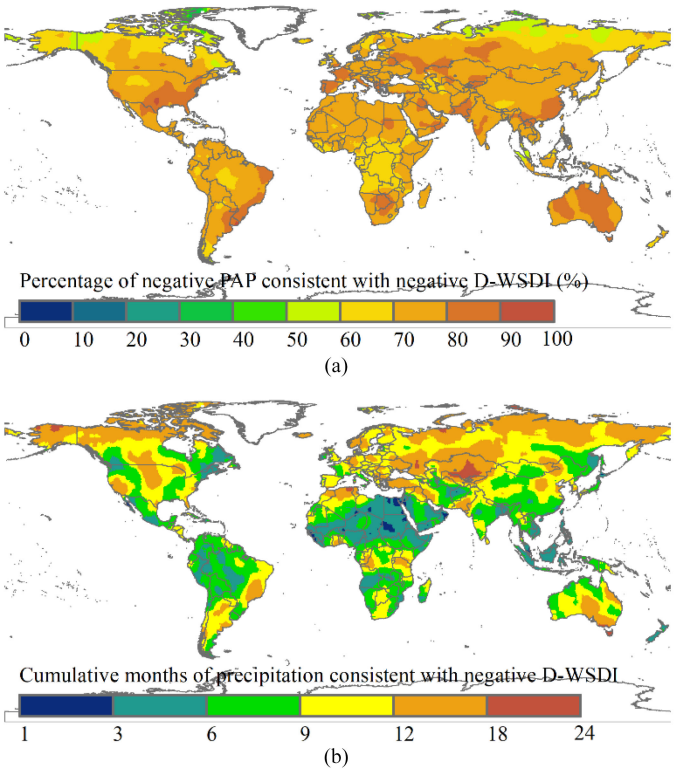

Fig. 5. (a) Maximum percentage of PAP <0 consistent with D-WSDI <0. (b) Corresponding cumulative months of precipitation.

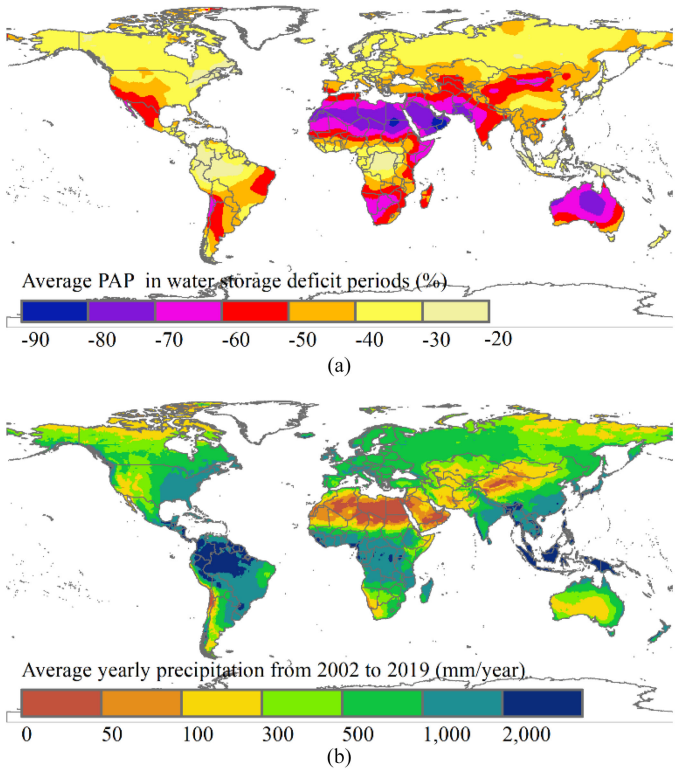

Fig. 6. (a) Average precipitation deficit percentage in water storage deficit periods. (b) GPM-based average yearly precipitation from 2002 to 2019.

The water storage deficit caused by drought in the low-latitude regions is more related to the precipitation deficit at the relatively short-term scales ($<$ 9 months), whereas high-latitude regions are more related to the relatively long-term scales ($>$ 9 months) [see Fig. 5(b)]. This may be attributed to the larger contribution of precipitation to TWS change in low-latitude basins, while larger contributions of evapotranspiration and runoff were identified for mid-and high-latitude basins [45]. Water storage deficit caused by drought seems to be better associated with the cumulative precipitation deficit for the duration between 6 and 13 months for most world regions, which agrees with the general knowledge that hydrological drought reflects a relatively long-lasting precipitation deficit [46], [47].

2) Magnitude of Precipitation Deficit Leading to Water Storage Deficit: Knowing how much precipitation can lead to the water storage deficit would be helpful for water resources management. The monthly negative PAP was used to calculate the mean precipitation deficit during negative D-WSDI periods. The magnitude of the precipitation deficit leading to the water storage deficit generally changes with latitude and rainfall (see Fig. 6). In tropical rainforest regions with high rainfall, a smaller precipitation deficit of about -20% will lead to a water storage deficit. In arid and semi-arid regions, the precipitation deficit leading to water storage is higher, up to -80%. The possible reason for this seemingly contradictory result is that a smaller PAP yields a more significant absolute water deficit in regions with high precipitation, while a larger PAP is needed to yield a significant absolute water shortage in drier regions. The terrestrial freshwater storage capacity is mainly related to surface dryness and wetness, and the vegetation cover, the arid and semiarid regions have higher freshwater storage capability, and wet areas show lower freshwater storage [48]. The mean percentage of precipitation deficit that can lead to the water storage deficit at the global scale is -43%, which is very consistent with the result in Section IV-A1, i.e., the mean monthly PAP during the drought period for all drought events is -44%.

C. Correlations of D-WSDI and Other Drought Indices

1) Comparisons of D-WSDI With Sun's WSDI and Zhao's DSI: Sun's WSDI is strongly related to Zhao's DSI, with r between them up to 0.988. Therefore, the spatial distribution of r between D-WSDI and Sun's WSDI at the pixel level is similar to that between D-WSDI and Zhao's DSI (see Fig. 7). The regions of D-WSDI inconsistent with Sun's WSDI and Zhao's DSI include North Africa, Western Asia, Central Asia, Western China, North China, the west and north of Canada, the Northwest of India, the central and southwest of North America, and the south of South America. In these regions, the long-term trend of TWS is generally decreasing because of arid climate or irrigated agriculture, leading to meet water requirements by exploiting groundwater, or glaciers retreating and melting due to the warming climate [24], [26], [49]–[53]. For those regions without the prominent long-term trend of TWS, D-WSDI has a similar performance to Sun's WSDI and Zhao's DSI.

2) Comparisons of D-WSDI and scPDSI and SPEI: The global mean r between D-WSDI and scPDSI is 0.38 [see Fig. 8(a)]. The areas with $r > 0.4$ are mainly located in the

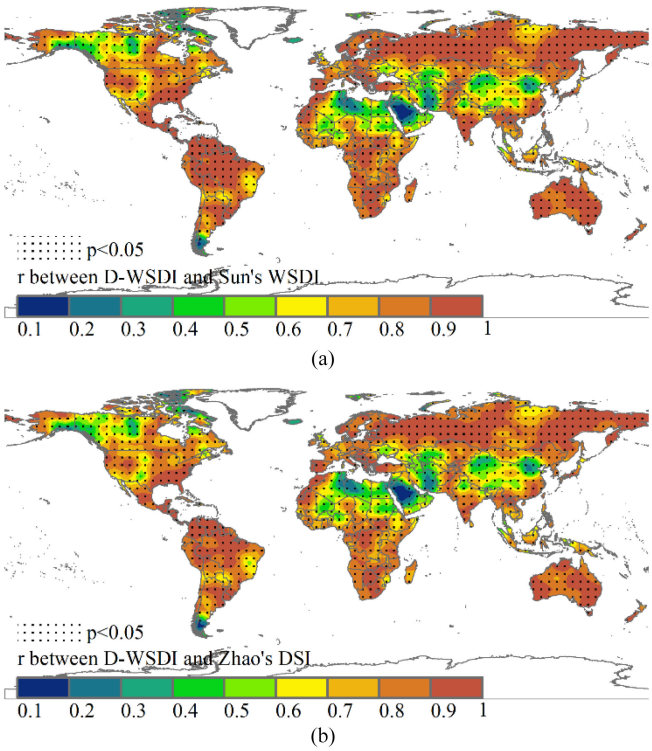

Fig. 7. Correlation coefficient (r) between D-WSDI and (a) Sun's WSDI and (b) Zhao's DSI from 2002 to 2019.

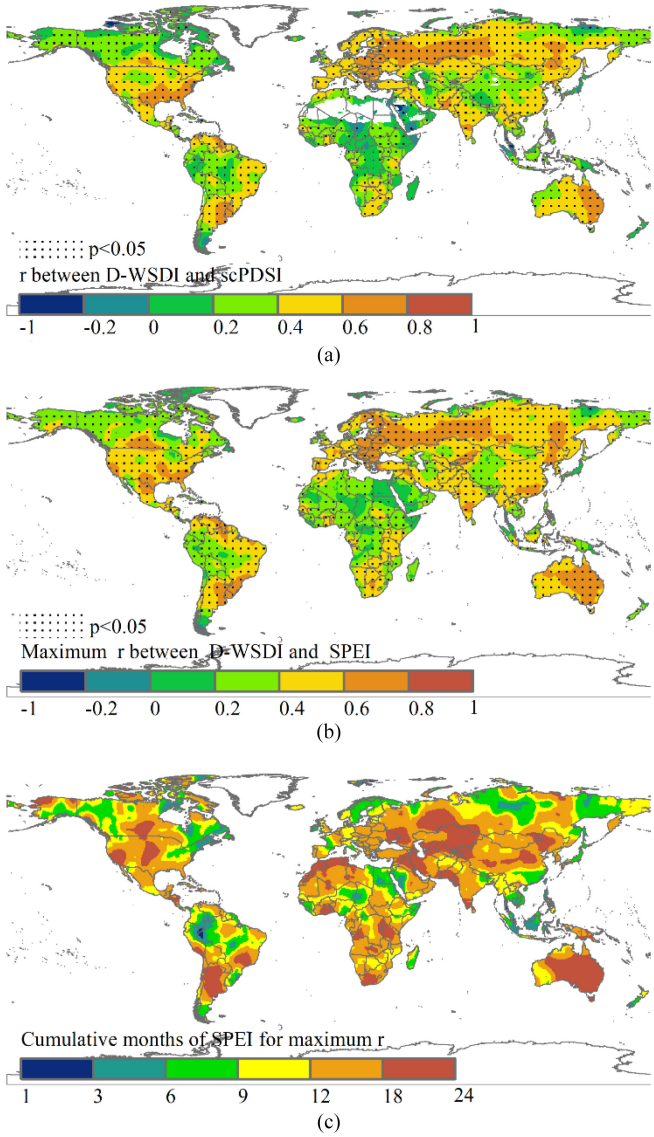

Fig. 8. (a) Correlation coefficient (r) between D-WSDI and scPDSI. (b) Maximum r between D-WSDI and SPEI. (c) Corresponding time scale of SPEI.

United States, the southeast of South America, Europe, the east of Asia, South Asia, the east of Australia, and a few regions in South Africa. The arid-semiarid regions, the equatorial regions, and the high-latitude regions with ice and snow cover generally have low r values. High r values imply that D-WSDI can detect drought with the same performance as scPDSI. In contrast, the low r values do not mean that D-WSDI has no skill in drought monitoring or that the drought does not lead to the water storage deficit, further discussed in next Section IV-D.

The r between D-WSDI and each SPEI of 1–24 months scales was calculated, and the maximum r is given in Fig. 8(b). The global mean value is 0.43. The spatial distribution of r is very similar to the one with scPDSI shown in Fig. 8(a), with r of 0.756 and $p < 0.01$. Larger r values between D-WSDI and SPEI may be attributed to using the maximum r, implying SPEI at the optimal time scale. The optimal time scale of SPEI was longer than 9 months for 80% of the world area, related to the long-term water budget, which is consistent with the results in a previous study [39].

Although the drought indices scPDSI and SPEI are often used for drought monitoring, we cannot expect a perfect match between D-WSDI and these indices. These indices deal with different variables related to drought, responding to various stages of drought evolution [16], [54]. GRACE is an independent or a complementary indicator for droughts [16], [20], [21]. The response of D-WSDI to global drought events given in Section IV-A2 can illustrate the excellent performance of D-WSDI for drought monitoring.

D. Time Series of D-WSDI and Other Drought Indices

We select some countries and subnational regions to analyze the inconsistencies between D-WSDI and other drought indices in the time series. These regions are Kenya and Congo (Democratic Republic of the Congo, DRC) in Africa, Tibet province in the west of China, and Shanxi province in North China (red boundaries in Fig. 1). Kenya is partly located upstream of the Nile River Basin and often suffers from drought. The Congo country is in the Congo River Basin, with abundant rainfall every year. The Nile River and the Congo River are two major rivers in Africa. The other two regions are in China. The Tibet province on the Tibetan plateau is the source area of Asian major rivers, with high elevations and relatively low temperatures. Shanxi province lies in the middle of the Yellow River Basin and the east of the Hai River Basin, with declining water storage and

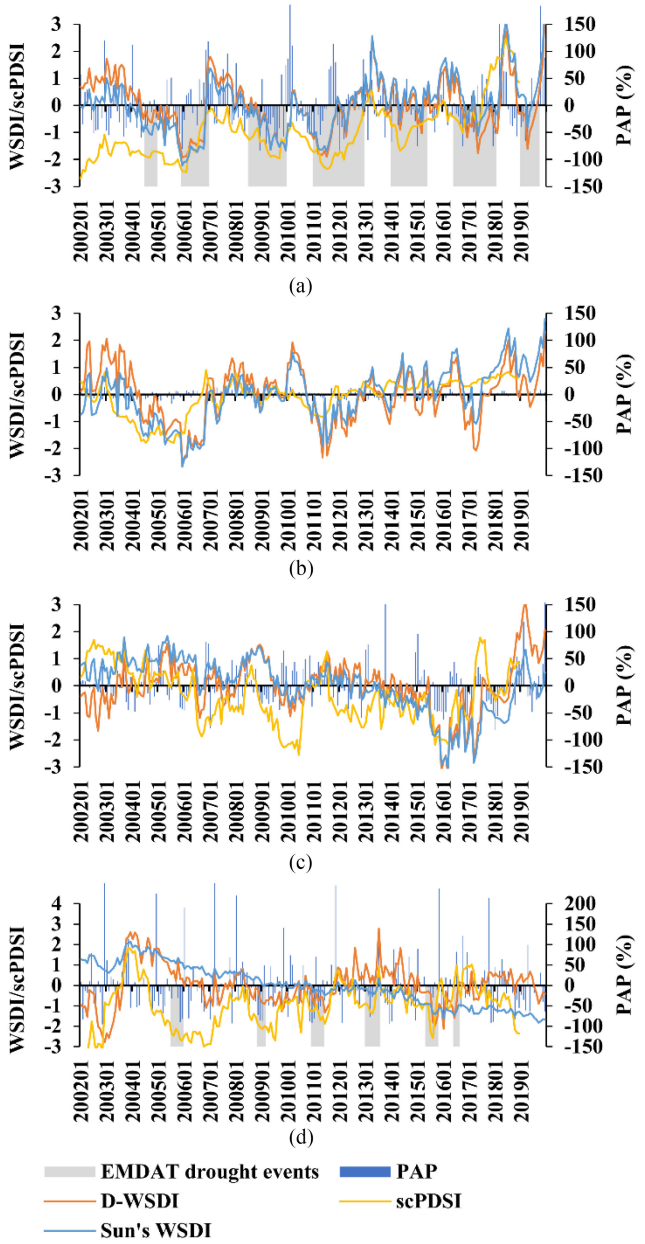

Fig. 9. Evolution of PAP, D-WSDI, and scPDSI for (a) Kenya, (b) Congo (DRC), (c) Tibet of China, and (d) Shanxi of China.

frequent drought. These regions are also that with relatively low r values in Fig. 7.

The evolution of D-WSDI and other drought indices of the four regions is shown in Fig. 9. The D-WSDI is generally consistent with Sun's WSDI, with a slightly increasing trend in Sun's WSDI for Kenya and Congo [see Figs. 9(a) and 9(b)] and a slight decrease in Tibet [see Fig. 9(c)]. The significant inconsistency between the D-WSDI and Sun's WSDI was for Shanxi province because of the decreasing water storage in this region [see Fig. 9(d)]. The groundwater depletion in North China has been paid wide attention because of the increasing water use demand [50], [51]. Drought can exacerbate water storage depletion. Sun's WSDI can reflect the declining trend of TWS rather than the impact of meteorological drought on water storage. D-WSDI can generally respond well to the extreme drought identified by scPDSI. The changes in D-WSDI closely correlate with PAP changes. It can be observed in Fig. 9 that when there is less precipitation, the values of D-WSDI decrease, and vice versa. Because of the difference between hydrological and meteorological droughts [47], the droughts identified by D-WSDI generally lag those expressed by PAP and scPDSI. Water storage is the result of the balance between water supplies (inputs) and demands (outputs). The water storage deficit in a given month not only depends on the precipitation of this month but also on the antecedent water storage and the water use in the given period. If there is sufficient water storage, even though poor precipitation or increasing water use for an extended period is, it will be possible that the water storage anomaly still keeps positive. If there has been a water storage deficit, the water storage anomaly may remain negative even though the abundant rainfall and declined water use are.

There are no drought records in the EM-DAT database for the two cases of Congo and Tibet, although there were occurrences of droughts. For the case of Congo [see Fig. 9(b)], D-WSDI follows the evolution of scPDSI well before 2013. After 2013, scPDSI is always positive, whereas precipitation anomaly and D-WSDI fluctuate with time. Significantly, an extreme water storage deficit appeared in 2017, but no evident precipitation negative anomaly or a negative scPDSI was observed. However, there was news on the drought leading to power shortage in Congo in 2017 (VOA news. DRC faces power shortage caused by drought; 2017.).[7] The negative precipitation anomaly was not significant in 2017, but the antecedent precipitation in 2016 was less than the average. The likely reason for the positive scPDSI value during this period is that surface vegetation may not suffer from water stress because of the use of surface or groundwater.

There are multiple occurrences of water storage deficit caused by droughts identified by D-WSDI from 2002 to 2019 in Tibet [see Fig. 9(c)]. The signal detected in 2002, 2006, 2010, and 2015–2018 are generally consistent with the drought period identified by scPDSI and always accompanied by negative precipitation anomalies. Although no drought in this province was recorded in the EM-DAT database, its neighboring regions, such as Yunnan, suffered from extreme droughts in 2001, 2010, and 2015, and Sichuan province experienced severe drought in 2006 [17], [55]–[59]. Zhu *et al.* [60] pointed out that this region experienced a long dry spell from 2011 to 2017, accompanied by a negative anomaly in low soil moisture. Except for the precipitation shortage, Tibet province holds a large water stock as glaciers and snow cover. With the increase in temperature accompanying drought, glaciers and snow may thaw and lead to a giant water outflow from this region. Therefore, in the areas covered by glaciers and snow, the drought or high temperature may aggravate the regional water storage deficit.

E. Uncertainties in D-WSDI

D-WSDI was calculated by the residual component of GRACE time-series data after removing the long-term trend

[7][Online]. Available: https://www.voanews.com/africa/drc-faces-power-shortage-caused-drought

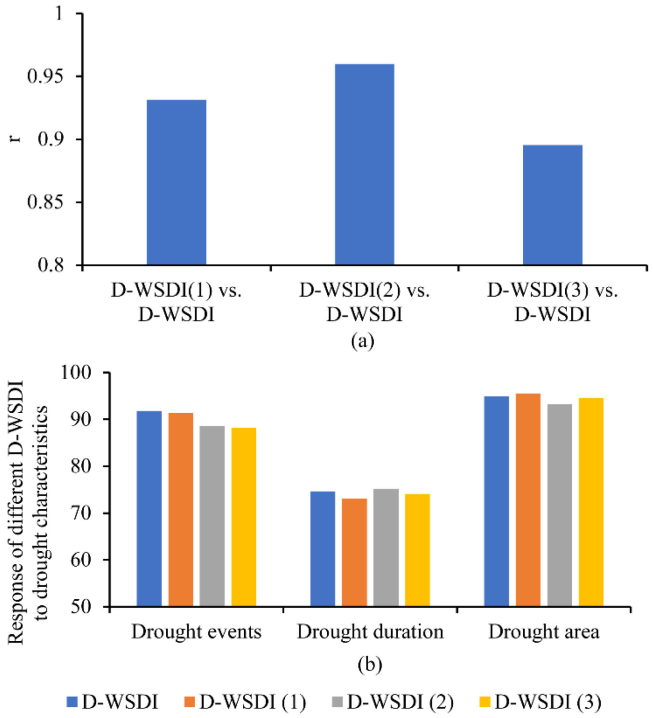

Fig. 10. (a) Comparison results of different D-WSDI, and (b) the response of different D-WSDI to drought characteristics of EM-DAT drought events (D-WSDI (1) was calculated by removing the long-term quadratic trend and stable season trend, D-WSDI (2) is by removing the long-term linear trend and unstable seasonal trend, and D-WSDI (3) is by removing the long-term quadratic trend and unstable seasonal trend).

and seasonal components in this study. The methods to obtain long-term and seasonal trends may impact the value D-WSDI. The quadratic trend and the unstable $S_{3\times3}$ seasonal filter (the symmetric three-term moving average of three-term averages) were applied to evaluate the uncertainties in calculating D-WSDI. The detail of $S_{3\times3}$ seasonal filter can be found in Appendix. Three combinations were set, i.e., the quadratic trend and stable season filter, the linear trend and unstable seasonal filter, and the quadratic trend and unstable seasonal filter. The comparison results of different D-WSDI are shown in Fig. 10(a). The D-WSDI calculated by removing the long-term linear trend and the unstable seasonal trend is strongly positively related to the results by removing the long-term linear trend and stable season trend, with $r > 0.95$. When the quadratic trend was used, the r value slightly was declined, but also greater than 0.9. When the quadratic trend and the unstable seasonal filter were simultaneously used, the r was nearly 0.9. The root-mean-square error among different D-WSDI is less than 0.5. The D-WSDI calculated by different methods showed a similar response to drought characteristics of EM-DAT drought events. They all identified near 90% drought events, 75% drought duration, and 95% drought area [see Fig. 10(b)]. These results indicated that the calculation for D-WSDI by the decomposition method is relatively stable.

As we know, some anomalies from surface deformation and those due to earthquakes or volcanic eruptions in GRACE fields [12], which are not easy to eliminate, are still the problem in D-WSDI. Additionally, this study applied the global drought events in the EM-DAT database to assess D-WSDI. The uncertainties in the EM-DAT database may be criticized. However, this study's main objectives are to explore the probability of drought leading to water storage deficit, clarify the magnitude and duration of precipitation anomaly to water storage deficit, and understand the performance of D-WSDI in drought monitoring. We believe these questions have been answered after this study.

V. Conclusion

Drought is a significant driver of the TWS deficit. This study proposed a D-WSDI by the time-series decomposition method. After removing the long-term and seasonal components, the residual part in the GRACE time series was used to calculate the D-WSDI to quantify the impact of drought on water storage deficit. In total, 92% of EM-DAT drought events between 2002 and 2019 led to a water storage deficit by the assessment based on D-WSDI, and the severity of the water storage deficit caused by drought increased with increasing drought duration. On average, 73% of the water storage deficit duration at the global scale was related to negative precipitation anomalies. In low-latitude regions, water storage deficit caused by drought is more correlative to negative precipitation anomalies at a relatively short-term scale (< 9 months) and longer duration in high-latitude regions. A smaller relative precipitation deficit of about -20% led to a water storage deficit in the areas with high rainfall. In comparison, a higher relative precipitation deficit of up to -80% was needed to induce a water storage deficit in the arid and semiarid regions. The apparent inconsistency between D-WSDI and previously developed GRACE-based indices in North Africa, Western Asia, Central Asia, Western China, North China, the west and north of Canada, the Northwest of India, the central and southwest of America, and the south of South America, appeared to be related to the long-term trends of TWS in these regions. D-WSDI is generally consistent with the commonly used drought indices scPDSI and SPEI but D-WSDI captured more drought events. The drought process is complex, and it impacts the whole process of the water cycle. Different variables of the water cycle have different responses to drought. The D-WSDI defined in this study can be used to qualify the water storage deficit caused by drought, and it is helpful for drought monitoring based on GRACE data and the analysis of the drivers of TWS deficit, and further to support sustainable use and management of water resources.

Appendix

Seasonal filter, also the moving average, is a way to estimate the seasonal component of a time series. A seasonal filter is a convolution of weights and observations made during past and future periods. In general, for a time series x_t ($t = 1, \ldots, N$), the seasonally smoothed observation at time $k + js$ ($j = 1, \ldots, N/s-1, k$ is the observations during the period, and s is the known periodicity of the seasonality) is

$$\tilde{s}_{k+js} = \sum_{l=-r}^{r} a_l x_{k+(j+l)s} \tag{A1}$$

with weights a_l such than $\sum_{l=-r}^{r} a_l = 1$.

The stable seasonal filter and the $S_{n\times m}$ seasonal filter are the two most commonly used seasonal filters. The stable seasonal filter assumes that the seasonal level does not change over time. Let n_k be the total of observations made in period k. The stable seasonal filter is given by

$$\tilde{s}_k = \frac{1}{n_k} \sum_{j=1}^{\frac{N}{s}-1} x_{k+js} \tag{A2}$$

for $k = 1, \ldots, s$, and $\tilde{s}_k = \tilde{s}_{k-s}$ for $k > s$.

The $S_{n\times m}$ seasonal filter is equivalent to taking a symmetric, unequally weighted moving average with $n+m-1$ terms, that is, $r = n+m-1$ in (A1). For example, an $S_{3\times 3}$ seasonal filter has five terms with weights (1/9, 2/9, 1/3, 1/9, 1/9).

REFERENCES

[1] J. S. Famiglietti, "Remote sensing of terrestrial water storage, soil moisture and surface waters," in *The State of the Planet: Frontiers and Challenges in Geophysics*, R. S. J. Sparks and C. J. Hawkesworth, Eds., vol. 150. Hoboken, NJ, USA: Wiley, 2004, pp. 197–207.

[2] J. Śliwińska, M. Wińska, and J. Nastula, "Terrestrial water storage variations and their effect on polar motion," *Acta Geophys.*, vol. 67, no. 1, pp. 17–39, Feb. 2019.

[3] F. Frappart, G. Ramillien, and J. Ronchail, "Changes in terrestrial water storage versus rainfall and discharges in the Amazon basin," *Int. J. Climatol.*, vol. 33, no. 14, pp. 3029–3046, Nov. 2013.

[4] T. Zhao *et al.*, "Soil moisture experiment in the Luan river supporting new satellite mission opportunities," *Remote Sens. Environ.*, vol. 240, 2020, Art. no. 111680.

[5] A. S. Richey *et al.*, "Quantifying renewable groundwater stress with GRACE," *Water Resour. Res.*, vol. 51, no. 7, pp. 5217–5238, 2015.

[6] B. D. Tapley *et al.*, "Contributions of GRACE to understanding climate change," *Nature Climate Change*, vol. 9, no. 5, pp. 358–369, May 2019.

[7] D. A. Wilhite, "Drought as a natural hazard: Concepts and definitions," in *Drought: A Global Assessment*, vol. I. London, U.K.: Routledge, 2000, pp. 3–18.

[8] A. AghaKouchak *et al.*, "Remote sensing of drought: Progress, challenges and opportunities," *Rev. Geophys.*, vol. 53, no. 2, pp. 452–480, 2015.

[9] H. West, N. Quinn, and M. Horswell, "Remote sensing for drought monitoring & impact assessment: Progress, past challenges and future opportunities," *Remote Sens. Environ.*, vol. 232, Oct. 2019, Art. no. 111291.

[10] B. R. Scanlon *et al.*, "Global evaluation of new GRACE mascon products for hydrologic applications," *Water Resour. Res.*, vol. 52, no. 12, pp. 9412–9429, 2016.

[11] A. Y. Sun, B. R. Scanlon, A. AghaKouchak, and Z. Z. Zhang, "Using GRACE satellite gravimetry for assessing large-scale hydrologic extremes," *Remote Sens.*, vol. 9, no. 12, Dec. 2017, Art. no. 1287.

[12] E. Forootan *et al.*, "Understanding the global hydrological droughts of 2003–2016 and their relationships with teleconnections," *Sci. Total Environ.*, vol. 650, pp. 2587–2604, Feb. 2019.

[13] W. Yu, Y. Li, Y. Cao, and T. Schillerberg, "Drought assessment using GRACE terrestrial water storage deficit in Mongolia from 2002 to 2017," *Water*, vol. 11, no. 6, 2019, Art. no. 1301.

[14] D. Zhang, X. Liu, and P. Bai, "Assessment of hydrological drought and its recovery time for eight tributaries of the Yangtze river (China) based on downscaled GRACE data," *J. Hydrol.*, vol. 568, pp. 592–603, Jan. 2019.

[15] H. Gerdener, O. Engels, and J. Kusche, "A framework for deriving drought indicators from the Gravity Recovery and Climate Experiment (GRACE)," *Hydrol. Earth Syst. Sci.*, vol. 24, no. 1, pp. 227–248, Jan. 2020.

[16] B. D. Vishwakarma, "Monitoring droughts from GRACE," *Front. Environ. Sci.*, vol. 8, 2020, Art. no. 584690.

[17] D. Long *et al.*, "Drought and flood monitoring for a large karst plateau in Southwest China using extended GRACE data," *Remote Sens. Environ.*, vol. 192, pp. 145–160, Dec. 2014.

[18] S. Z. Yirdaw, K. R. Snelgrove, and C. O. Agboma, "GRACE satellite observations of terrestrial moisture changes for drought characterization in the Canadian Prairie," *J. Hydrol.*, vol. 356, no. 1, pp. 84–92, Jul. 2008.

[19] H. Yi and L. Wen, "Satellite gravity measurement monitoring terrestrial water storage change and drought in the continental United States," *Sci. Rep.*, vol. 6, no. 1, Jan. 2016, Art. no. 19909.

[20] M. Zhao, A. Geruo, I. Velicogna, and J. S. Kimball, "Satellite observations of regional drought severity in the continental United States using GRACE-based terrestrial water storage changes," *J. Climate*, vol. 30, no. 16, pp. 6297–6308, 2017.

[21] M. Zhao, A. Geruo, I. Velicogna, and J. S. Kimball, "A global gridded dataset of GRACE Drought Severity Index for 2002–14: Comparison with PDSI and SPEI and a case study of the Australia millennium drought," *J. Hydrometeorol.*, vol. 18, no. 8, pp. 2117–2129, 2017.

[22] Z. Sun, X. Zhu, Y. Pan, J. Zhang, and X. Liu, "Drought evaluation using the GRACE terrestrial water storage deficit over the Yangtze River Basin, China," *Sci. Total Environ.*, vol. 634, pp. 727–738, Sep. 2018.

[23] A. C. Thomas, J. T. Reager, J. S. Famiglietti, and M. Rodell, "A GRACE-based water storage deficit approach for hydrological drought characterization," *Geophys. Res. Lett.*, vol. 41, no. 5, pp. 1537–1545, 2014.

[24] V. Humphrey, L. Gudmundsson, and S. I. Seneviratne, "Assessing global water storage variability from GRACE: Trends, seasonal cycle, subseasonal anomalies and extremes," *Surv. Geophys.*, vol. 37, no. 2, pp. 357–395, Mar. 2016.

[25] S.-M. Hosseini-Moghari, S. Araghinejad, K. Ebrahimi, and M. J. Tourian, "Introducing modified total storage deficit index (MTSDI) for drought monitoring using GRACE observations," *Ecol. Indicators*, vol. 101, pp. 465–475, Jun. 2019.

[26] S.-M. Hosseini-Moghari, S. Araghinejad, K. Ebrahimi, Q. Tang, and A. AghaKouchak, "Using GRACE satellite observations for separating meteorological variability from anthropogenic impacts on water availability," *Sci. Rep.*, vol. 10, no. 1, Sep. 2020, Art. no. 15098.

[27] X. Liu, X. Feng, P. Ciais, B. Fu, B. Hu, and Z. Sun, "GRACE satellite-based drought index indicating increased impact of drought over major basins in China during 2002–2017," *Agricultural Forest Meteorol.*, vol. 291, Sep. 2020, Art. no. 108057.

[28] F. W. Landerer *et al.*, "Extending the global mass change data record: GRACE Follow-On instrument and science data performance," *Geophys. Res. Lett.*, vol. 47, no. 12, 2020, Art. no. e2020GL088306.

[29] F. Fatolazadeh and K. Goïta, "Mapping terrestrial water storage changes in Canada using GRACE and GRACE-FO," *Sci. Total Environ.*, vol. 779, Jul. 2021, Art. no. 146435.

[30] D. N. Wiese, F. W. Landerer, and M. M. Watkins, "Quantifying and reducing leakage errors in the JPL RL05M GRACE mascon solution," *Water Resour. Res.*, vol. 52, no. 9, pp. 7490–7502, 2016.

[31] V. Humphrey and L. Gudmundsson, "GRACE-REC: A reconstruction of climate-driven water storage changes over the last century," *Earth Syst. Sci. Data*, vol. 11, no. 3, pp. 1153–1170, 2019.

[32] Z. Sun, D. Long, W. Yang, X. Li, and Y. Pan, "Reconstruction of GRACE data on changes in total water storage over the global land surface and 60 basins," *Water Resour. Res.*, vol. 56, no. 4, 2020, Art. no. e2019WR026250.

[33] Y. Zhong, W. Feng, V. Humphrey, and M. Zhong, "Human-induced and climate-driven contributions to water storage variations in the Haihe River Basin, China," *Remote Sens.,* vol. 11, no. 24, 2019, Art. no. 3050.

[34] J. Tan, G. J. Huffman, D. T. Bolvin, and E. J. Nelkin, "IMERG V06: Changes to the morphing algorithm," *J. Atmos. Ocean. Technol.*, vol. 36, no. 12, pp. 2471–2482, 2019.

[35] G. J. Huffman *et al.*, "Integrated multi-satellite retrievals for the global precipitation measurement (GPM) mission (IMERG)," in *Satellite Precipitation Measurement: Volume 1*, V. Levizzani, C. Kidd, D. B. Kirschbaum, C. D. Kummerow, K. Nakamura, and F. J. Turk, Eds., Cham: Springer, 2020, pp. 343–353.

[36] W. C. Palmer, "Meteorological drought," Office Climatology, US Weather Bureau, Washington, DC, USA, Research Paper No. 45, p. 58, 1965.

[37] N. Wells, S. Goddard, and M. J. Hayes, "A Self-Calibrating Palmer Drought Severity Index," *J. Climate*, vol. 17, no. 12, pp. 2335–2351, Jun. 2004.

[38] G. van der Schrier, J. Barichivich, K. R. Briffa, and P. D. Jones, "A scPDSI-based global data set of dry and wet spells for 1901–2009," *J. Geophys. Res. Atmos.*, vol. 118, no. 10, pp. 4025–4048, 2013.

[39] S. M. Vicente-Serrano, S. Beguería, J. I. López-Moreno, M. Angulo, and A. El Kenawy, "A new global 0.5 gridded dataset (1901–2006) of a multiscalar drought index: Comparison with current drought index datasets based on the Palmer Drought Severity Index," *J. Hydrometeorol.*, vol. 11, no. 4, pp. 1033–1043, 2010.

[40] E. B. Dagum, "Time series modeling and decomposition," *Statistica*, vol. 70, no. 4, pp. 433–457, Dec. 2010.

[41] P. J. Brockwell, *Introduction to Time Series and Forecasting*, 2nd ed. New York, NY, USA: Springer, 2002.

[42] G. G. Mace, C. Jakob, and K. P. Moran, "Validation of hydrometeor occurrence predicted by the ECMWF model using millimeter wave radar data," *Geophys. Res. Lett.*, vol. 25, no. 10, pp. 1645–1648, 1998.
[43] "WMO guidelines on generating a defined set of national climate monitoring products," World Meteorol. Org. (WMO), Geneva, Switzerland, WMO-No. 1204, 2017.
[44] *Grades of Meteorological Drought*, China Nat. Standard GB/T 20481-2017, 2017.
[45] Y. Zhang, B. He, L. Guo, J. Liu, and X. Xie, "The relative contributions of precipitation, evapotranspiration, and runoff to terrestrial water storage changes across 168 river basins," *J. Hydrol.*, vol. 579, Dec. 2019, Art. no. 124194.
[46] A. F. Van Loon, "Hydrological drought explained," *WIREs Water*, vol. 2, no. 4, pp. 359–392, 2015.
[47] W. Wang, M. W. Ertsen, M. D. Svoboda, and M. Hafeez, "Propagation of drought: From meteorological drought to agricultural and hydrological drought," *Adv. Meteorol.*, vol. 2016, pp. 1–5, 2016.
[48] E. Zhu and X. Yuan, "Global freshwater storage capability across time scales in the GRACE satellite era," *Adv. Atmos. Sci.*, vol. 38, no. 6, pp. 905–917, Jun. 2021.
[49] B. R. Scanlon *et al.*, "Groundwater depletion and sustainability of irrigation in the US High Plains And Central Valley," *Proc. Nat. Acad. Sci. USA*, vol. 109, no. 24, pp. 9320–9325, 2012.
[50] Q. Tang, X. Zhang, and Y. Tang, "Anthropogenic impacts on mass change in North China," *Geophys. Res. Lett.*, vol. 40, no. 15, pp. 3924–3928, 2013.
[51] Z. Huang *et al.*, "Subregional-scale groundwater depletion detected by GRACE for both shallow and deep aquifers in North China plain," *Geophys. Res. Lett.*, vol. 42, no. 6, pp. 1791–1799, 2015.
[52] D. Long *et al.*, "Have GRACE satellites overestimated groundwater depletion in the Northwest India aquifer?," *Sci. Rep.*, vol. 6, Apr. 2016, Art. no. 24398.
[53] M. Rodell *et al.*, "Emerging trends in global freshwater availability," *Nature*, vol. 557, no. 7707, pp. 651–659, May 2018.
[54] Z. Amin, S. Rehan, N. Bahman, and I. K. Faisal, "A review of drought indices," *Environ. Rev.*, vol. 19, pp. 333–349, 2011.
[55] L. Jia, G. Hu, J. Zhou, and M. Menenti, "Assessing the sensitivity of two new indicators of vegetation response to water availability for drought monitoring," *Proc. SPIE*, vol. 8524, 2012, Art. no. 85241A.
[56] S. Abbas, J. E. Nichol, F. M. Qamer, and J. Xu, "Characterization of drought development through remote sensing: A case study in central Yunnan, China," *Remote Sens.*, vol. 6, no. 6, pp. 4998–5018, 2014.
[57] X. Q. Zhang and Y. Yamaguchi, "Characterization and evaluation of MODIS-derived Drought Severity Index (DSI) for monitoring the 2009/2010 drought over southwestern China," *Nat. Hazards*, vol. 74, no. 3, pp. 2129–2145, Dec. 2014.
[58] W. Lin, C. Wen, Z. Wen, and H. Gang, "Drought in Southwest China: A review," *Atmos. Ocean. Sci. Lett.*, vol. 8, no. 6, pp. 339–344, Jan. 2015.
[59] Y. Li, Z. Wang, Y. Zhang, X. Li, and W. Huang, "Drought variability at various timescales over Yunnan Province, China: 1961–2015," *Theor. Appl. Climatol.*, vol. 138, no. 1, pp. 743–757, Oct. 2019.
[60] Y. Zhu *et al.*, "Spatio-temporal variations in terrestrial water storage and its controlling factors in the Eastern Qinghai-Tibet Plateau," *Hydrol. Res.*, vol. 52, no. 1, pp. 323–338, 2020.

Jing Lu received the Ph.D. degree in geographic information system from the Institute of Geographic Sciences and Natural Recourses Research, Chinese Academy of Sciences, Beijing, China, in 2014.

She is currently an Assistant Researcher with the State Key Laboratory of Remote Sensing Science, Aerospace Information Research Institute, Chinese Academy of Sciences. Her research focuses on remote sensing-based evapotranspiration estimation, drought monitoring, water resource evaluation, and global climate change.

Li Jia (Member, IEEE) received the B.S. degree in dynamic meteorology from the Beijing College of Meteorology, Beijing, China, in 1988, the M.Sc. degree in atmospheric physics from the Chinese Academy of Sciences, Beijing, in 1997, and the Ph.D. degree in environmental science from Wageningen University, Wageningen, The Netherlands, in 2004.

She is currently a Professor with the State Key Laboratory of Remote Sensing Science, Aerospace Information Research Institute, Chinese Academy of Sciences. Her research interests include the study of earth observation and its applications in hydrometeorology, water resource, agriculture, and climate change.

Jie Zhou received the B.S. degree in geographic information system from the China University of Geoscience, Wuhan, China, in 2010, and the Ph.D. degree in cartographic and geographic information system from the Institute of Remote Sensing and Digital Earth, Chinese Academy of Sciences, Beijing, China, in 2016.

From 2013 to 2015, he was a visiting scholar with the Delft University of Technology, Delft, The Netherlands. He is currently an Associate Professor with the Central China Normal University, Wuhan. His research interests include the time-series analysis of remote sensing data, drought monitoring using earth observations, and global environmental change.

Min Jiang received the Ph.D. degree in physical geography from the Institute of Geographic Sciences and Natural Recourses Research, Chinese Academy of Sciences, Beijing, China, in 2019.

He is currently an Assistant Researcher with the State Key Laboratory of Remote Sensing Science, Aerospace Information Research Institute, Chinese Academy of Sciences. His research interests include vegetation change and drought monitoring, land use and cover change, and environmental effects.

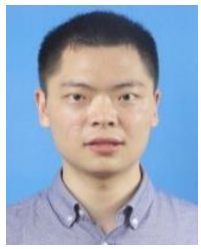

Yulong Zhong received the Ph.D. degree in geodesy and survey engineering from the Institute of Geodesy and Geophysics, Chinese Academy of Sciences, Beijing, China, in 2018.

He is currently an Assistant Professor with the China University of Geosciences (Wuhan), Wuhan, China. His research interests focus on applying satellite gravimetry, including the groundwater storage change estimates, regional evapotranspiration estimate from GRACE, and separation of climate change and human activity in GRACE terrestrial water storage.

Massimo Menenti received the Ph.D. degree in environmental sciences from the University of Wageningen, Wageningen, The Netherlands, in 1984.

He is currently a foreign expert at the Aerospace Information Research Institute, Chinese Academy of Sciences, Beijing, China. His research interests include the retrieval of land surface parameters from remote sensing, the heat and water exchanges between the land and atmosphere, time-series analysis of satellite remote sensing observations, and the application of remote sensing in hydrology, agriculture, water resources, crop yields, and climate models.